Journal of Luminescence 203 (2018) 7–15

Contents lists available at ScienceDirect

Journal of Luminescence

journal homepage: www.elsevier.com/locate/jlumin

Solid state photoluminescence studies of $[EuL^nH_2(NO_3)_3](H_2O)_x$ macrocyclic complexes with Schiff base ligands

Ricardo C. de Santana[a,*], Pablo A. Fuentealba[b,c], Lauro J.Q. Maia[a], Verónica Paredes-García[c,d], Daniel Aravena[e], Diego Venegas-Yazigi[c,e], Jorge Manzur[c,f], Evgenia Spodine[b,c]

[a] Instituto de Física, Universidade Federal de Goiás, Goiânia (GO), Brazil
[b] Facultad de Ciencias Químicas y Farmacéuticas, Universidad de Chile, Santiago, Chile
[c] Centro para el Desarrollo de Nanociencias y Nanotecnología, CEDENNA, Santiago, Chile
[d] Departamento de Ciencias Químicas, Universidad Andrés Bello, Santiago, Chile
[e] Facultad de Química y Biología, Universidad de Santiago de Chile, USACH, Santiago, Chile
[f] Facultad de Ciencias Físicas y Matemáticas, Universidad de Chile, Santiago, Chile

ARTICLE INFO

Keywords:
Eu^{III} complexes
Macrocyclic ligands
Luminescence
Judd-Ofelt parameters

ABSTRACT

Three Eu^{III} macrocyclic complexes $[EuL^nH_2(NO_3)_3](H_2O)_x$ based on the ligands derived from 2-hydroxy-5-methyl-1,3-benzenedicarbaldehyde and three different amines: *o*-phenylenediamine, Eu-OPDA; ethylenediamine, Eu-EDA; and 1,3-diaminopropane, Eu-DAP have been synthesized via a metal template reaction. Eu-EDA and Eu-DAP showed metal based emission; for the Eu-OPDA complex these luminescent properties were not observed. From the photoluminescence emission measurements from ~13 to 300 K, the R/O = I ($^5D_0 \rightarrow {}^7F_2$)/I ($^5D_0 \rightarrow {}^7F_1$) ratio, together with two intensity parameters (Ω_2 and Ω_4), radiative lifetimes (τ_R) and branching ratios ($\beta_{0\,J'}$) were calculated based on the Judd-Ofelt theory, for Eu-EDA and Eu-DAP. While the behavior of these parameters for the Eu-DAP complex is temperature dependent, these remain constant for Eu-EDA. The temperature dependence observed for the Eu-DAP complex indicates that for temperatures below 120 K, the local symmetry of the Eu^{III} center is modified, as compared to the environment of the same metal center at room temperature.

1. Introduction

Coordination compounds based on lanthanide ions have been intensively studied because of their interesting magnetic properties, such as single molecule magnet behavior [1], and photophysical properties [2]. Moreover, particular interest exists for the complexes of lanthanides with iminophenol macrocyclic Schiff base type ligands [3–9]. Since the lanthanide (III) ions have low absorption coefficients in the UV–visible spectrum [10], due to the fact that the absorption are Laporte forbidden, the amount of absorbed radiation corresponding to the excitation of the *4f* orbitals is limited, and the subsequent luminescence is weak. This has been overcome with the use of the "antenna effect", that is, by excitation of a sensitizing chromophore of the ligand of the corresponding molecular lanthanide (III) coordination compound. In this way, the luminescence in the lanthanide complexes occurs through energy transfer pathways involving ligand (S1) to ligand (T1) to the emitting levels of the LnIII [11]. Nevertheless, a few examples exist in which a dominant singlet pathway becomes evidente [12,13]. Thus, when the intersystem crossing rate is smaller than 10^{11} s^{-1}, a singlet transfer mechanism has been reported to occur [14,15].

In relation to the spectroscopic properties, europium (III) compounds have been investigated by several research groups, and different reviews have appeared in the literature [16–18]. The interest in europium (III) complexes lies in the fact that the lifetime of emission from the excited state is in the range of milliseconds, which makes these compounds interesting for different applications, such as luminescent sensors for pH, pO2, and selected anions [19]. as NMR shift reagents [20,21], and biomedical applications [22–27]. The difficulty to control the coordination sphere of the rare earth ions is evident, since these display high and variable coordination numbers. Due to the versatility of the coordination number of the lanthanide ions, the variety of structures associated to these ions is enormous. As the physical properties of the lanthanide ions depend greatly on the structural aspects of the corresponding compounds, in the case of europium (III) compounds the fine structure and the relative intensities of the emission bands can serve to infer the local environment of the metal center, that is, the coordination polyhedron and point group symmetry.

In order to study the "antenna effect" of a family of macrocyclic

* Corresponding author.
E-mail address: santana@ufg.br (R.C. de Santana).

https://doi.org/10.1016/j.jlumin.2018.06.022
Received 2 January 2018; Received in revised form 6 June 2018; Accepted 8 June 2018
Available online 15 June 2018

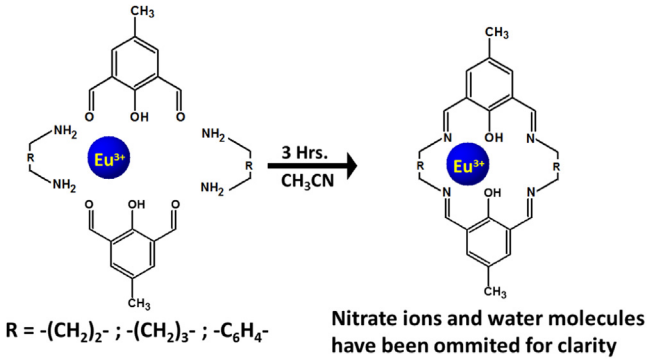

Scheme 1. Representation of the synthesis of the macrocyclic complexes.

ligands derived from 2-hydroxy-5-methyl-1,3-benzenedicarbaldehyde and three different amines Ln: (n = 1) o-phenylene-diamine, (n = 2) ethylenediamine, or (n = 3) 1,3-diaminopropane, we herein report the optical properties of a family of mononuclear europium (III) macrocyclic complexes, $[EuL^nH_2(NO_3)_3](H_2O)_x$, hereafter called Eu-OPDA, Eu-EDA and Eu-DAP, respectively.

2. Experimental

2.1. Materials and syntheses

Scheme 1 shows the syntheses of mononuclear [2 + 2] macrocyclic complexes, $[EuL^nH_2(NO_3)_3](H_2O)_x$ at room temperature by the metal template reaction using acetonitrile as reaction solvent, following the synthetic method reported by Suresh Kumar and Alexander [28]. To a solution of 2-hydroxy-5-methyl-1,3-benzenedicarbaldehyde (1 mmol in 50 mL acetonitrile), a solution of the europium (III) salt was added (0.5 mmol europium nitrate hexahydrate in 30 mL acetonitrile). Finally, a solution of the corresponding amine in the same solvent was slowly added, and left to react for 3 h at room temperature. The obtained solid was separated by filtration, washed with acetonitrile and chloroform, and dried in vacuum. The purity of the obtained complexes was confirmed by FTIR spectra and C, H, and N analyses. Anal. Calc. for Eu-OPDA, $[EuL^1H_2(NO_3)_3](H_2O)_2$, $[C_{30}\ H_{28}\ N_7\ O_{13}Eu]$ C, 42.56; H, 3.33; N, 11.58%. Found C, 42.95; H, 3.53; N, 11.38%. For Eu-DAP, $[EuL^2H_2(NO_3)_3]H_2O$, $[C_{24}H_{30}N_7O_{12}Eu]$ C, 37.90; H, 3.98; N, 12.89% Found C, 37.0; H, 3.6; N, 12.3%. For Eu-EDA, $[EuL^3H_2(NO_3)_3]H_2O$, $[C_{22}H_{26}N_7O_{12}Eu]$ C, 36.08; H, 3.58; N, 13.39%. Found C, 35.9; H, 3.94; N, 12.51%. The corresponding FTIR spectra are given as Supplementary material (Fig. S1).

The yttrium (III) complexes, used as optical blanks for the photoluminescent studies [29] were synthesized by the same procedure. Anal. Calc. for Y-OPDA $[C_{30}\ H_{28}\ N_7\ O_{13}Y]$ C, 45.99; H, 3.60; N, 12.51%. Found C, 46.4; H, 3.6; N, 12.30%. For Y-DAP $[C_{24}\ H_{32}N_7\ O_{13}Y]$ C, 40.29; H, 4.51; N, 13.70%. Found C, 40.93; H, 4.69; N, 14.02%. For Y-EDA $[C_{22}\ H_{28}N_7\ O_{13}Y]$ C, 38.44; H, 4.11; N, 14.26%. Found C, 38.98; H, 4.26; N, 14.39%.

2.2. Physical measurements

Elemental analyses were performed using a Flash 2000 Instrument. Fourier transform infrared spectra (FTIR) were recorded on a Thermo Scientific Nicolet iS5, with an ATR iD5 accessory, in the range 4000–650 cm^{-1}. Diffuse reflectance spectra of $EuL^nH_2(NO_3)_3(H_2O)_x$ samples were obtained on a PerkinElmer Lambda WB1050 spectrophotometer, equipped with a Praying Mantis diffuse reflection accessory. The relation between the diffuse reflectance of the sample (R_∞), absorption coefficient (K) and scattering coefficient (S) is given by the Kubelka–Munk function $F(R_\infty)$ [30]:

$$F(R_\infty) = (1-R_\infty)^2/(2R_\infty) = K/S \quad (1)$$

where $R_\infty = R_{sample}/R_{reference}$. The band gap E_g and absorption coefficient α of a direct band gap semiconductor is related through the Tauc relation [30]:

$$\alpha h\nu = A(h\nu - E_g)^{1/2} \quad (2)$$

where A is a proportionality constant. When the powder scatters in perfectly diffuse manner, the absorption coefficient K becomes equal to 2α. Considering the scattering coefficient S as constant with respect to wavelength, and using Eqs. (1) and (2), the following expression can be written:

$$(F(R_\infty)h\nu)^2 = A(h\nu - E_g)^{1/2} \quad (3)$$

From the plot of $(F(R_\infty)\ h\nu)^2$ versus $h\nu$, the value of E_g was obtained by extrapolating the linear fitted region to $(F(R_\infty)\ h\nu)^2 = 0$ [30].

PL emission spectra of the solid samples were measured using a Horiba–Jobin Yvon spectrofluorimeter, Model Fluorolog–3 (FL3–221), under excitation at 369 nm (λ_{exc} = 369 nm) and 394 nm (λ_{exc} = 394 nm) from a 450 W Xe lamp, and the detection by a Hamamatsu photomultiplier tube, operating from 260 nm to 850 nm. The used excitation and emission slits were of 2 nm. PL emission was corrected for the spectral response of the monochromators and the detector using a typical correction spectrum provided by the manufacturer. All low–temperature spectra were obtained using a closed cycle cryostat model CS202AI–X15 (ARS Cryo), with the temperature being monitored by a Lake Shore model 332 controller. Spectroscopic studies were performed on powder samples.

2.3. Computational details

All DFT calculations were performed using the FHI–X15 (ARS Cryo), with the temperature being monitored aims code [31]. Geometry optimizations were performed using the PBE functional [32] in conjunction with the default 'light' basis set. To account for scalar relativistic effects, the ZORA Hamiltonian was included [33]. The coordination environment around the Eu^{III} centers in Eu–OPDA, Eu–EDA and Eu–DAP was analyzed using the SHAPE 2.1 program [34,35]. The SHAPE program allows for the comparison of arbitrary shapes to ideal geometries for coordination environments, providing an unambiguous value for the deviation between both shapes (the S parameter). In this approach, the zero value for S means a perfect match between ideal and target geometries, while an increasing number is related with larger deviations.

3. Results and discussion

3.1. Structural models

Even though single crystals were not obtained, structural models can be proposed for the studied complexes. Complexes with a C2 backbone, Eu–EDA and Eu–OPDA, can be considered as planar with the metal center coordinated above the plane defined by the macrocyclic ligand, while Eu–DAP may be envisaged as having the ligand forming an angle, due to the flexibility of the C3 backbone of the diaminopropane moiety. Literature gives examples of this folding, as in the case of the anhydrous complex, $[La(DAP)(NO_3)_3]$, whose structure was obtained by single X–ray diffraction, and reported by Bag et al. [36], or the one obtained by Duncan et al. for $[Eu–TIDP–Pr–tBu(NO_3)_3]\cdot 3CH_3CN$ [9]. In both cases "butterfly–like" structures are obtained. The latter is also based on the 1,3–diaminopropane macrocyclic ligand, TIDP–Pr–tBu being similar to the DAP macrocyclic ligand, only that the methyl substituent of the used dicarbaldehyde was replaced by a *tert*–Bu one. In $[Eu–TIDP–Pr–tBu(NO_3)_3]\cdot 3CH_3CN$ the Eu^{III} center has a coordination number of 10; the coordination sphere being formed by two phenolate oxygen atoms and two imine nitrogen atoms derived

from the 1,3-diaminopropane fragment, and three bidentate nitrate anions. Considering the information available in literature for lanthanide complexes with similar ligands, we assumed that the studied europium (III) ion was coordinated to four donor atoms from the macrocyclic ligand and six oxygen atoms from three bidentate nitrate ions.

The FTIR spectra of the studied Eu^{III} complexes (Fig. S1) are characterized by the absence of the peak at 1680 cm^{-1} corresponding to unreacted aldehyde, which together with the elemental analyses data, gives evidence of the purity of the obtained complexes. The vibration of the –C=N– group of the formed macrocyclic ligand is present at *ca.* 1650 cm^{-1}. Both Eu-DAP and Eu-EDA show the C=N vibration at higher energies (1646 and 1652 cm^{-1} respectively) as compared to Eu-OPDA (1627 cm^{-1}). These data can be explained by the fact that the latter has a higher degree of delocalization in the macrocyclic ligand, as compared to the ligands derived from aliphatic amines. The presence of the *o*-phenylenediamine moiety in the Eu-OPDA complex is assessed by the C-H vibration at 757 cm^{-1}, for *ortho* substituted benzene rings. Besides, the FTIR spectra of all compounds are characterized by the absence of an intense band of the ionic nitrate at 1384 cm^{-1}, proving that all nitrate are coordinated to the europium ion. Bands at 1484 and 1293 cm^{-1} for Eu-OPDA ($\Delta\nu$ = 191 cm^{-1}), 1482 and 1302 cm^{-1} for Eu-DAP ($\Delta\nu$ = 180 cm^{-1}), and 1482 and 1300 cm^{-1} for Eu-EDA ($\Delta\nu$ = 182 cm^{-1}) should be assigned to bidentate nitrate ions. Makhinson et al. [8] recently reported the synthesis and characterization of the same compound, Eu-EDA that presents two bands at ~1490 and ~1300 cm^{-1}, and a $\Delta\nu$ value close to 190 cm^{-1}, ascribing these bands to bidentate nitrate ions [37].

To analyze changes in the first coordination sphere induced by the different macrocyclic ligands, optimized geometries of the three complexes were obtained by means of DFT calculations (see computational details section for details). Based on the FTIR data, structural models for the proposed coordination environments were constructed for Eu-DAP, Eu-EDA and Eu-OPDA, considering four donor atoms from the macrocyclic ligand and three bidentate NO_3^-. In all cases, stable energy minimum structures were obtained. Despite the similarities of the studied molecules, noticeable differences in the relaxed geometries were found, which can be related with the distinctive geometrical features of each macrocyclic ligand. The macrocyclic ligand provides four coordination positions for the Eu^{III} ion, in a half-sandwich like conformation. The conformation of these four donor atoms heavily depends on the macrocycle: Eu-DAP shows N-Eu-O angles of 93° and 114° (where N and O are the coordinating atoms at opposite positions of the square formed by the Eu-coordinating donor atoms of the macrocycle), Eu-EDA presents angles of 110° and 87° and Eu-OPDA shows angles of 94° and 98°. As expected, the macrocycles with a shorter spacer (EDA and OPDA) are related with less obtuse angles due to their limited flexibility, locating the Eu^{III} ion further out-of-plane in comparison to DAP macrocycle (1.620 Å, 1.674 Å and 1.753 Å for Eu-DAP, Eu-EDA and Eu-OPDA, respectively).

Macrocycle folding angles are defined by the vectors passing through the carbon atom of the methyl group at the para-position of the aromatic rings and the oxygen donor atoms (see Fig. 1 for a graphical description). If these two vectors are coplanar, the folding angle (α) can be straightforwardly described by building the triangle formed by the O-O segment and the projection of both vectors. DFT optimized structures are close to this coplanar condition, with C-O-O-C dihedral angles of 7.5° (Eu-DAP), 9.5° (Eu-EDA) and 1.7° (Eu-OPDA), confirming the appropriate definition of α. Folding angles are calculated to be 118.7°, 121.4° and 131.5° for Eu-DAP, Eu-EDA and Eu-OPDA, respectively. As expected, the OPDA ligand is closer to 180° due to its larger aromaticity in comparison to DAP and EDA. Three NO_3^- ligands bind to Eu^{III} at the opposite face with respect to the macrocyclic ligand. All compounds (Fig. 2a-c) present a coordination number of 10, as all NO_3 ligands result bicoordinated as was initially proposed. SHAPE measurements indicate a reasonable similitude to the sphenocorona shape (S = 3.49, 3.47 and 3.53 for Eu-DAP, Eu-EDA and Eu-OPDA, respectively), while Eu-OPDA is also close to a tetradecahedron (2:6:2) (S = 3.06). In all cases, the two originally phenolic protons are found to be closer to the uncoordinated N donor atoms of the macrocycle, irrespective of the initial geometry employed in the geometry optimizations. In this way, the macrocycle is coordinating as a neutral zwitterionic ligand. All these structural features are consistent with FTIR analysis and crystal structures of similar compounds reported in literature [9].

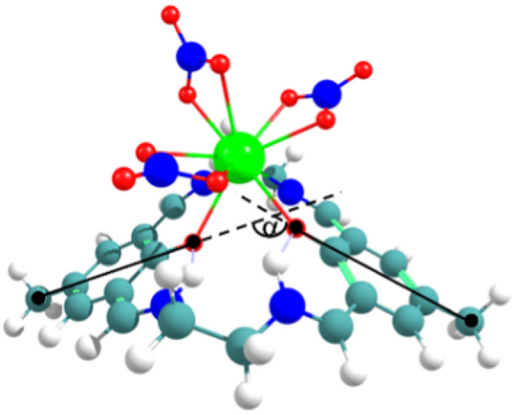

Fig. 1. Definition of the folding angle (α) for the macrocycles. Atoms employed for angle measurements are indicated with black circles.

3.2. Absorption properties

The absorption properties of the obtained complexes were studied in solution and in solid state. For the studies done in solution, a DMSO:H_20 (1:2) mixture was used. Fig. 3a shows the absorption spectra of the Eu^{III} complexes, and Fig. 3b the corresponding of the Y^{III} complexes which were used as optical blanks. It is possible to observe that the spectra of the complexes derived from aliphatic amines are similar, presenting a band a 410 nm with a shoulder close to 400 nm, while the spectrum of the complex derived from o-phenylenediamine shows two bands, at 350 and 420 nm. Table 1 summarizes the corresponding maxima and the absorption coefficients. The fact that these bands are present in both europium and yttrium complexes proves that these are intraligand processes.

Fig. 4a and S2a shows the diffuse reflectance spectra (DRS) of all studied Eu^{III} and Y^{III} complexes, which were recorded in the range of 400–1800 nm, using finely ground powder samples. The spectra of the yellow Eu-DAP, Eu-EDA, Y-DAP and Y-EDA present the band edge absorption near 400–460 nm, in contrast with those of the brown Eu-OPDA and Y-OPDA, where the band edge is near 560–650 nm. From the spectra in Fig. 4b-d, and S2b-d, and using the Kubelka-Munk theory [30,38] described above, the optical band gap was determined from the solid state spectra using Eqs. (1)–(3). The band gap E_g for all samples was obtained from the graphs $[F(R_\infty)h\nu]^2$ *vs.* $h\nu$ (Fig. 4b-d and S2b-d), and the values are 2.16 eV for Eu–OPDA (Fig. 4b), 2.66 eV for Eu – DAP (Fig. 4c), 2.66 eV for Eu–EDA (Fig. 4d), 1.94 eV for Y–OPDA (Fig. S2b), 2.67 eV for Y–DAP (Fig. S2c), 2.59 eV for Y–EDA (Fig. S2d) respectively.

Both groups of complexes present the same trend of calculated band gap, where E_g(OPDA) < E_g(DAP) ≤ E_g(EDA). Since the band gap can be defined as the energy difference between the HOMO and the LUMO, the structure design should allow the control of the E_g magnitude, thus modifying the optical properties [39–41]. For example, among the few values of E_g for Eu^{III} complexes reported in literature, the octacoordinated [Eu(TTA)$_3$ phen] complex has a value of 3.26 eV [39].

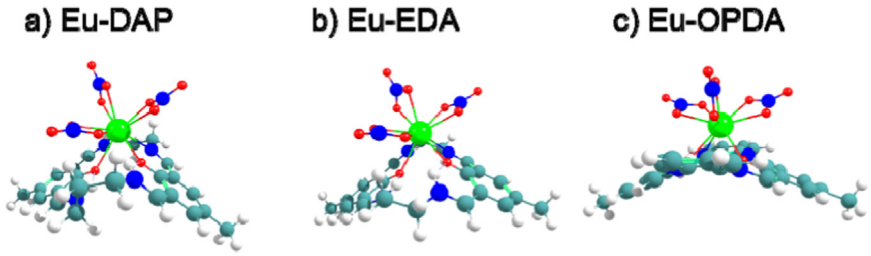

Fig. 2. DFT optimized structural models for (a) Eu–DAP, (b) Eu–EDA and (c) Eu–OPDA. Color code: Eu (green); O (red); N (blue); C (light blue) and H (white). (For interpretation of the references to color in this figure legend, the reader is referred to the web version of this article.)

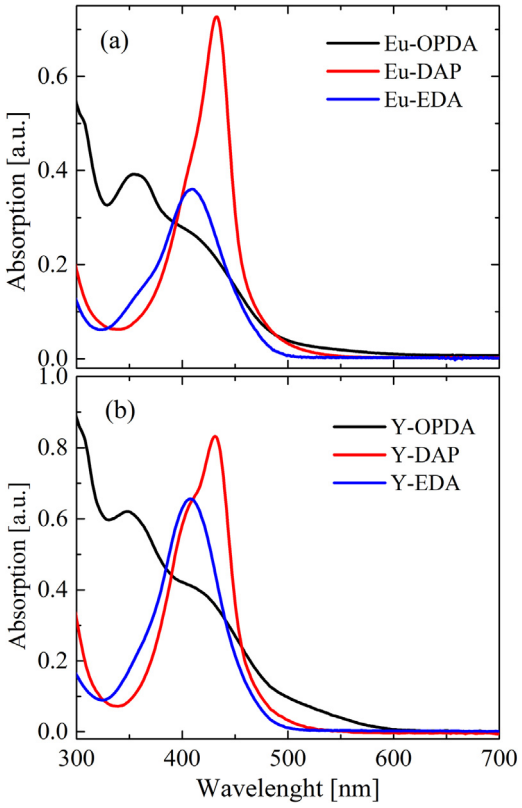

Fig. 3. Absorption spectra of the (a) Eu^{III} and (b) Y^{III} complexes.

Table 1
λ and ε obtained from the absorption spectra in solution.

Complex	λ_{Abs} (nm)	ε (M^{-1} cm^{-1})
Eu–EDA	360	Sh
	410	1.24×10^4
Eu–DAP	407	Sh
	432	1.81×10^4
Eu–OPDA	355	1.45×10^4
	410	9.45×10^3
Y–DAP	414	Sh
	431	1.62×10^4
Y–EDA	360	Sh
	410	1.06×10^4
Y–OPDA	350	1.22×10^4
	420	7.36×10^3

3.3. Photoluminescence spectra and Judd–Ofelt parameters

Fig. 5a depicts the excitation spectra of all complexes measured in the 17,000– 30,000 cm^{-1} range and normalized to the same intensity span, acquired monitoring at room temperature the hypersensitive $^5D_0 \rightarrow {}^7F_2$ Eu^{III} transition at 16,155 cm^{-1} (619 nm). It was possible to identify in all spectra a broad band centered at 27,142 cm^{-1} (368 nm), and narrower bands centered at 17,508 cm^{-1} (571 nm) for Eu–OPDA, 18,358 cm^{-1} (545 nm) for Eu–DAP and 19,008 cm^{-1} (526 nm) for Eu–EDA, certainly related to ligand excitation in each complex, showing the existence of the antenna effect.

Fig. 6b shows the emission spectra of the studied complexes, obtained by excitation at 369 nm (300 K). The ligand emission band in the case of Eu–EDA (from ~ 15,000 to ~ 21,000 cm^{-1}) is more intense than the Eu^{III} luminescence (from ~ 14,000 to ~ 17,500 cm^{-1}). This phenomenon may be due to the fact that the triplet state of the EDA ligand is very close in energy to the emissive state of europium (III), and produces an extensive vibrationally mediated back energy transfer at room temperature [8]. The spectra of Eu–OPDA, Eu–EDA and Eu–DAP present broad and intense lines in the blue-green region at 25,000–18,000 cm^{-1} (400–555 nm), assigned to intraligand transitions. These were confirmed by the emission measurements of Y–EDA, Y–OPDA and Y–DAP complexes, where only the emission from the ligand is observed (Fig. S3) [29,42]. Moreover, the spectra of Eu–DAP and Eu–EDA also have sharp lines in the 17,000 – 14,000 cm^{-1} (590–715 nm), attributed to $^5D_0 \rightarrow {}^7F_{0,1,2,3,4}$ Eu^{III} transitions. They are more prominent in the Eu–DAP spectrum in comparison with Eu–EDA spectrum, because in this last species the emission from the EDA ligand is much more intense than for the DAP ligand, indicating that in the Eu–DAP complex the ligand transfers the absorbed energy to the emitting $^5D_0$ level of Eu^{III} more efficiently than EDA and OPDA ligands. No emission of Eu^{III} ions is observed in the Eu–OPDA spectrum, which may be attributed both to the position of the band edge absorption near 560–650 nm, as observed in the diffuse reflectance spectra (Fig. 4a), and the emission of the ligand.

Upon excitation of Eu–EDA and Eu–DAP with 394 nm radiation, metal centered emission bands were also observed. Fig. 6 shows the temperature dependence of the emission spectra in the 13–298 K temperature range for Eu–DAP, where the bands become more resolved as the temperature is lowered. As pointed by de Jesus et al. [43], the presence of the forbidden $^5D_0 \rightarrow {}^7F_0$ transition in the emission spectrum is indicative that the Eu^{III} ions are located on a symmetry site without an inversion center. The $^5D_0 \rightarrow {}^7F_6$ transition could not be detected experimentally in any of the recorded spectra, since it lies at lower energies in the infrared region and is beyond the recorded region.

The emission bands correspond exclusively to the Eu^{III} $^5D_0 \rightarrow {}^7F_{0,1,2,3,4}$ transitions, indicating an efficient energy transfer from the ligand to the trivalent rare earth ion. The fact that at lower temperature the spectra are more resolved, can be attributed to the reduction of electron–phonon coupling that affects the peak positions, widths and intensity [44]. Regardless of the temperature, the spectra are dominated by the hypersensitive $^5D_0 \rightarrow {}^7F_2$ electric dipole (ED) transition, as usually occurs when the Eu^{III} occupies a site without an inversion center, since the Laporte rule is relaxed due to odd parity terms in the ligand field Hamiltonian [10,45]. The barycenter of all observed transitions at each temperature for Eu–DAP is constant within the experimental error. Lowering the temperature, the spectra of both complexes, Eu–EDA and Eu–DAP, present different Stark splitting in some of the Eu^{III} emission bands. As pointed by Carlos et al. [46], the presence of

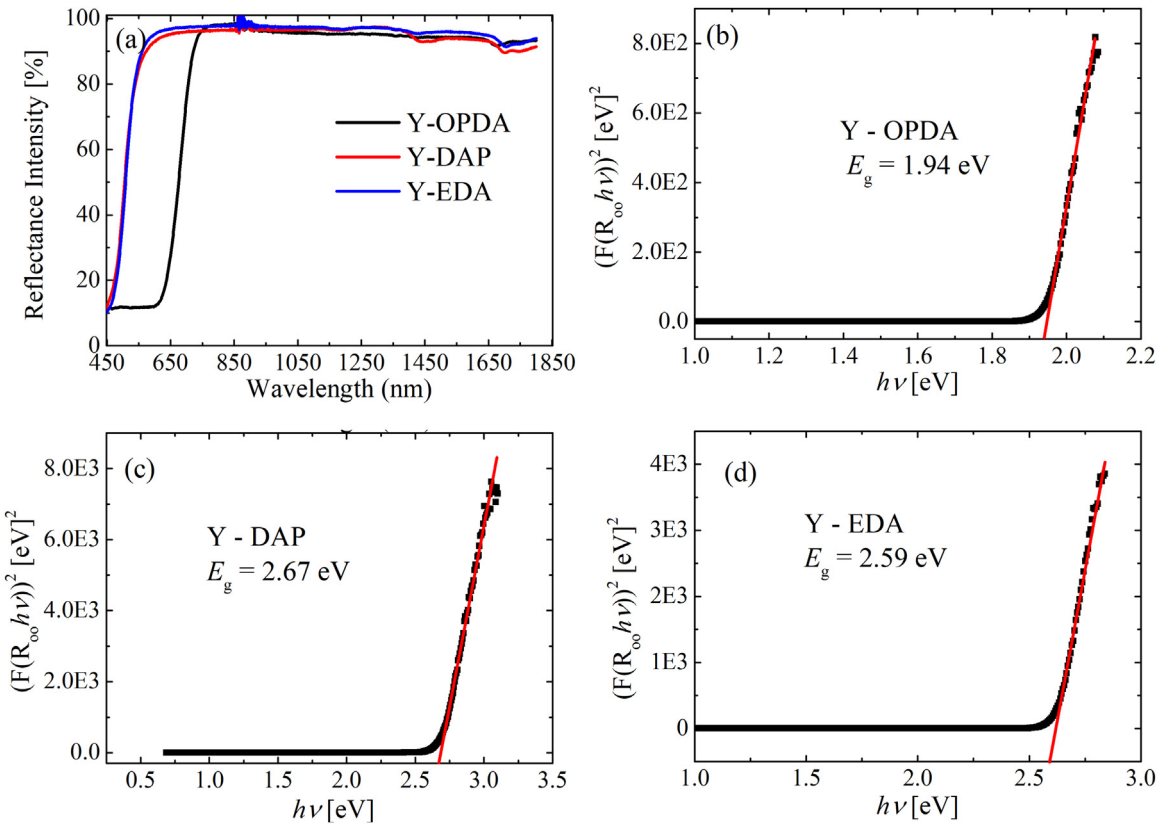

Fig. 4. (a) Powder diffuse reflectance spectra (DRS) of Eu^{III} complexes, taken at room temperature. (b) – (d) shows the determination of the band gap energy of the complexes.

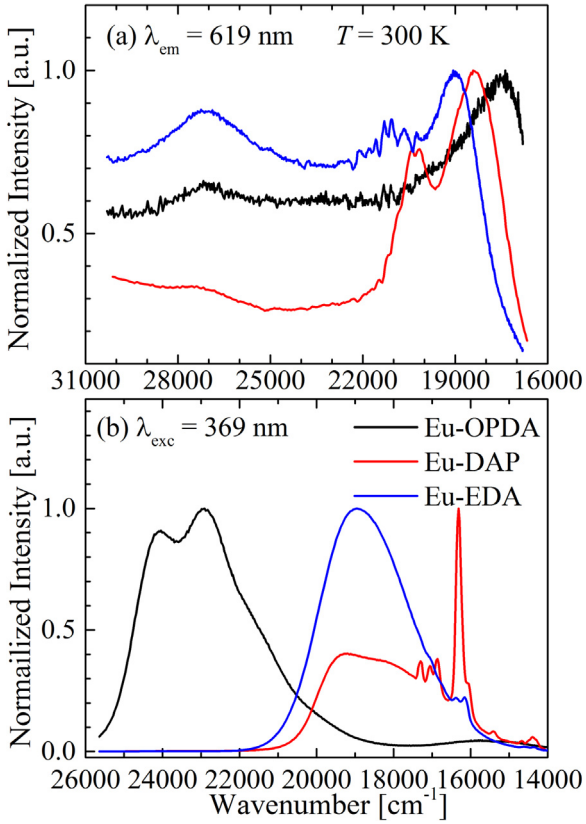

Fig. 5. (a) Excitation spectrum monitoring the $^5D_0 \rightarrow {}^7F_2$ transition (λ_{em} = 619 nm) and (b) emission spectra under excitation at 369 nm and room temperature.

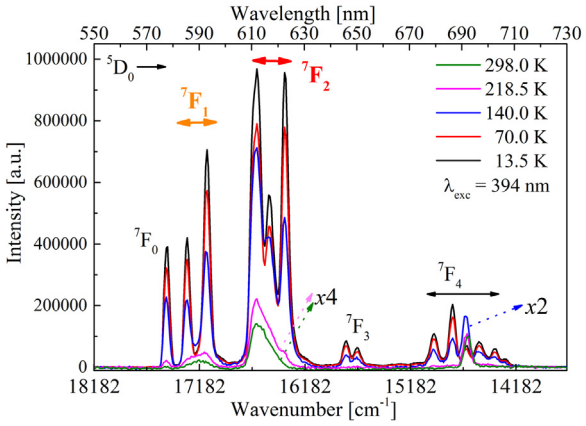

Fig. 6. Photoluminescence spectra of Eu–DAP under excitation at 394 nm, collected between 13.5 K and 298.0 K. For the better visualization of the recorded spectra, at 140.0 K were multiplied by 2, while those taken at 298.0 K and 218.5 K were multiplied by a factor 4.

$^5D_0 \rightarrow {}^7F_{0,3}$ Eu^{III} transitions, together with the J–degeneracy splitting and the observation of the different number of split components over the measured wavenumber range (see Fig. S4), indicate different low-symmetry environments for the Eu^{III} cations in both emitting complexes.

The $^5D_0 \rightarrow {}^7F_1$ transition centered at 16,863 cm^{-1} (orange, O) has a magnetic dipole nature (MD) and is not affected by the ligand environment. Thus, it serves as an internal reference in contrast with the following transition $^5D_0 \rightarrow {}^7F_2$ centered at 16,430 cm^{-1} (red, R), which is extremely sensitive to ligand environment and to the coordination sphere symmetry [43]. The ratio of these two bands is taken as a

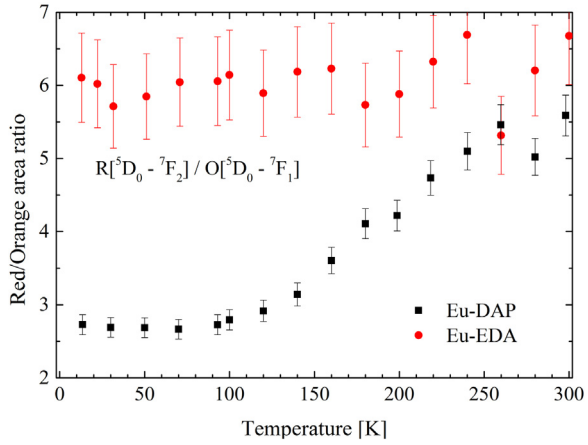

Fig. 7. R/O area ratio for Eu–DAP and Eu–EDA samples as a function of the temperature.

measurement of the symmetry of the coordination environment. Fig. 7 shows the dependence of R/O = $I(^5D_0 \rightarrow {}^7F_2)/I(^5D_0 \rightarrow {}^7F_1)$ ratio as a function of the temperature for Eu–DAP and Eu–EDA. For Eu–DAP this R/O ratio is constant from 13 to 120 K being 2.7, but it increases almost linearly from 2.7 to 5.6 between 120 and 298 K, while for Eu–EDA this ratio remains almost constant (~6.0) in the whole temperature range. This behavior for Eu–DAP may be due to the possible changes in the local Eu^{III} environment when the temperature is lowered; the local environment remaining unaltered below 120 K. The R/O = 2.7 value at 13 K for Eu–DAP is consistent with a Eu^{III} in a more symmetrical site when compared with R/O = 5.6 at 293 K. Besides, the R/O values also suggest a higher degree of Eu–O bond covalency for Eu-DAP at lower temperature [47–49]. In contrast, the R/O ratio of 6.0 for Eu–EDA in the whole studied temperature range, indicates a low degree of covalency for the Eu–donor atom bonds, with the Eu^{III} occupying an asymmetric coordination center [47]. Thus, this observed difference between the R/O ratios *vs.* temperature can be attributed to the presence of the used ligands with different flexibility.

The spectral properties of Eu–DAP and Eu–EDA in the temperature range of 13 to 298 K were investigated using the Judd–Ofelt (JO) theory, which is an efficient tool to analyze *f–f* transitions [50,51]. The Judd-Ofelt theory is used in treating the emission spectra of glasses and crystalline species. In order to use this theory and calculate the Judd-Ofelt parameters, some approximations have to be made. We have assumed that the ground Stark levels are equally populated, even at low temperatures, since this assumption remains valid for ions in low symmetry sites as is the case of the europium(III) centers in the studied complexes [52–54].

Intensity parameters Ω_2 and Ω_4, the radiative emission rate (A_{rad}), the radiative lifetime (τ_{rad}) and the branching ratios β_{02} and β_{04} were calculated by using data from emission spectra, associated with the $^5D_0 \rightarrow {}^7F_2$ and $^5D_0 \rightarrow {}^7F_4$ transitions. These data were compared with those of the MD transition, $^5D_0 \rightarrow {}^7F_1$. The least square fitting method was used to calculate the barycenter and the area for all emission bands at each temperature. For the Eu–EDA spectra, where the Eu^{III} emissions appear superimposed with the ligand emission, the baselines of all spectra were extracted before the barycenter and area calculations. The estimated uncertainties in the areas were < 5% for the strongest lines and ~ 7–10% for the weakest. It is possible to express the spontaneous emission probabilities for $^5D_0 \rightarrow {}^7F_{0,1,2,3,4}$ transitions of the Eu^{III} through the following equation:[10]

$$A\left(^5D_0 \rightarrow {}^7F_J\right) = \frac{4e^2\omega^3}{3\hbar c^3}\frac{n_0(n_0^2+2)}{9}\sum_{\lambda}\Omega_\lambda \langle {}^7F_J\|U^{(\lambda)}\|{}^5D_0\rangle^2 \quad (4)$$

where e is the electron charge, n_0 is the index of refraction of the host, ω is the frequency of the transition, $\hbar$ is the Planck's constant, Ω_λ are the Judd–Ofelt intensity parameters [50,51] and $\langle {}^7F_J\|U^{(\lambda)}\|{}^5D_0\rangle^2$ is the reduced matrix element for $\lambda = J = 0$, 2 and 4, given by Carnall et al. [55] For the particular case of Eu^{III} the total radiative decay rate, A_{rad}, can be written in terms of the area under the emission curves S_{0J} as:

$$A_{rad} = \frac{A_{01}hc\omega_{01}}{S_{01}}\sum_{J=0}^{6}\frac{S_{0J}}{hc\omega_{0J}} \quad (5)$$

where A_{01} is the spontaneous decay rate for the $^5D_0 \rightarrow {}^7F_1$ transition given by $A_{01} = A'_{01}n^3$ with $A'_{01} = 14.65\ s^{-1}$ in vacuum. The intensity parameters Ω_λ were calculated with the relation [10]:

$$\Omega_\lambda = \frac{3h}{64\pi^4e^2\bar{\omega}^3c^3}\frac{9}{n(n^2+2)}\frac{1}{|\langle {}^7F_J\|U^{(\lambda)}\|{}^5D_0\rangle|^2}A_{0J} \quad (6)$$

$|\langle {}^7F_J\|U^{(\lambda)}\|{}^5D_0\rangle|^2$ are the squared reduced matrix elements whose values are 0.0032 and 0.0023 for J= 2 and 4, respectively [52,54]. Due to the poor relative intensities of the $^5D_0 \rightarrow {}^7F_{5,6}$ transitions we have neglected these values. The predicted radiative lifetime τ_{rad} is given by the inverse of the total area under the emission curves, $\tau_{rad} = 1/A_{rad}$, and the branching ratios are given by $\beta_{0J'} = A_{0J'}/A_{rad}$, being $J' = 1$, 2 or 4.

The temperature dependence of the Ω_λ intensity parameters (λ = 2 and 4), the radiative lifetime τ_R and the β_{01}, β_{02} and β_{04} are shown in Fig. 8a, b and c, for Eu–DAP and Eu–EDA, respectively. In Table 2 some values of these parameters for selected temperatures are summarized. Analyzing Fig. 8a, an initial point to be noted is the relatively high values of the Ω_2 parameter for Eu–EDA over the entire temperature

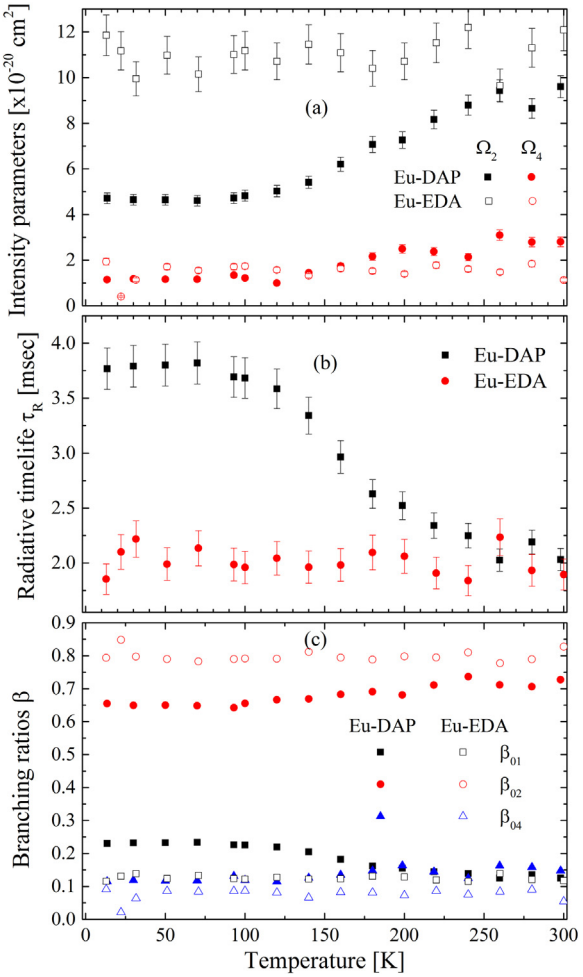

Fig. 8. Evolution of the (a) Judd–Ofelt intensity parameters, Ω_2 and Ω_4; (b) radiative lifetimes; and (c) branching ratios values as a function of temperature for Eu–DAP and Eu–EDA compounds.

Table 2
Radiative decay rates A_{rad}, lifetime τ_{rad}, Ω_2 and Ω_4 Judd–Ofelt parameters and β_{0J} branching ratios for selected temperatures.

Eu–DAP								Eu–EDA							
Temp [K]	A_{rad} [s^{-1}]	τ_{rad} [ms]	Ω_2 [10^{-20} cm^2]	Ω_4	β_{01} [%]	β_{02}	β_{04}	Temp [K]	A_{rad} [s^{-1}]	τ_{rad} [ms]	Ω_2 [10^{-20} cm^2]	Ω_4	β_{01} [%]	β_{02}	β_{04}
13.5	265.4	3.77	4.71	1.15	0.23	0.65	0.11	13.0	539.7	1.85	11.82	1.93	0.12	0.79	0.09
50.0	263.1	3.80	4.64	1.16	0.23	0.65	0.12	51.1	502.6	1.99	10.98	1.71	0.12	0.79	0.09
70.0	261.7	3.32	4.61	1.16	0.23	0.65	0.12	70.8	468.6	2.13	10.15	1.55	0.13	0.78	0.08
140.0	299.3	3.34	5.41	1.44	0.21	0.67	0.13	140.0	509.8	1.96	11.45	1.32	0.12	0.81	0.07
180.0	380.5	2.63	7.07	2.16	0.16	0.69	0.15	180.0	477.2	2.10	10.41	1.52	0.13	0.79	0.08
240.1	444.8	2.25	8.79	2.13	0.14	0.74	0.12	240.0	544.0	1.84	12.19	1.61	0.12	0.81	0.07
298.0	492.4	2.03	9.61	2.80	0.12	0.73	0.15	300.0	527.8	1.89	12.09	1.13	0.12	0.83	0.05

range, when compared to the values of Eu–DAP. The Ω_2 parameter behavior as a function of temperature for both complexes is similar to the R/O values, as observed in Figs. 7 and 8a. So, the Ω_2 values indicate that the Eu^{III} ion is in a temperature independent environment in Eu–EDA, as compared to that of Eu–DAP [43,56]. This behavior may be interpreted as a consequence of the sensibility of the $^5D_0 \rightarrow {}^7F_2$ transition to the local symmetry of Eu^{III}. Moreover, the calculated Ω_2 parameter values at room temperature are far from the values reported for Eu^{III} β–diketonate compounds, such as $[Eu(btfa)_3(4,4'–bpy)(EtOH)]$ and $[Eu(tta)_3{\cdot}2H_2O]$ with $\Omega_2 = 30.9 \times 10^{-20}$ and 40.0×10^{-20} cm^2, respectively [57,58]. These data suggest that the dynamic coupling mechanisms are less efficient in the studied compounds than in the β–diketonates.

Another aspect to be considered from the temperature dependence of Ω_2 for both samples is that their moderately high values at room temperature (Table 2) should also be taken as indicative of a certain degree of covalent character of the Eu^{III}–ligand bonds in both samples at this temperature [10,59]. Moreover, as the Ω_2 values for Eu–DAP decrease with the lowering of temperature this can be associated with the formation of a more polarizable structure. On the other hand, the Ω_4 values for both samples are almost independent of temperature [60].

The asymmetry around rare–earth ions and their polarization are determined by the Ω_2 parameter, while Ω_4 parameter depends on long-range effects [61]. The higher Ω_2 values at low temperatures for Eu-EDA indicate that the Eu^{III} ion has a more asymmetric coordination sphere than for Eu–DAP. At room temperature both have almost the same Ω_2 values, which are corroborated by the R/O ratio (Fig. 7). The lower Ω_4 values, as compared to Ω_2 values for both complexes in the whole temperature range implies that $^5D_0 \rightarrow {}^7F_2$ transition efficiency increases, resulting in a red emission of Eu^{III} ions.

Fig. 8a shows that the radiative lifetime (τ_R) is constant for Eu–EDA over all the temperature range, while for Eu–DAP the τ_R value is constant, ~ 3.8 ms, between 13.5 K and 120 K and decreasing to ~2.1 ms at 298 K. These values are in good correlation with the Ω_2 values, being sensitive to the structural changes in the vicinity of the lanthanide ion (short range effect) [60]. The radiative lifetime (τ_R) at room temperature for Eu–DAP and Eu–EDA (Table 2 and Fig. 8b) are similar, with values 2.03 and 1.89 ms, respectively. However, an uncommon temperature evolution of τ_R for Eu–DAP is observed, indicating that τ_R is dependent on the environment of the Eu^{III} ions. Changes in the radiative lifetime values are also related to phonon coupling between Eu^{III} and host lattice, being similar to those reported by Berry et al. [62] for $Eu(thd)_3$ single crystals, where $(thd)_3 \equiv$ tris(2,2,6,6–tetramethyl–3,5–heptanedionato). However, for this system the sudden change in the τ_R values occurs near room temperature, while for the Eu–DAP complex it occurs at ~120 K, Fig. 8b. This strong temperature dependence of the $^5D_0$ lifetime for Eu–DAP is unusual for Eu^{III} ions in molecular europium (III) complexes. Concerning the τ_R results for Eu–EDA, the calculated value is 2.13 ms at 70 K, being greater than the value measured by Makhinson et al. [8] for EuL (L= EDA) in methanolic solution, $\tau = 1.083(5)$ ms at 77 K. We attribute this difference between our system and the one reported in literature to the effect of the medium. In general, luminescence studies in solution depend on both the concentration and the type of used solvent, a fact that can introduce changes in the local coordination of the lanthanide ion by modifying the first coordination sphere and the emission processes.

Analyzing the $\beta_{0J'}$ branching ratios listed in Table 2, we observe that the values at room temperature follow different trends, $\beta_{02} > \beta_{04} > \beta_{01}$ and $\beta_{02} > \beta_{01} > \beta_{04}$, for Eu–DAP and Eu–EDA respectively, being in the order of relative intensities $^5D_0 \rightarrow {}^7F_2 > {}^7F_4 > {}^7F_1$ for Eu–DAP and $^5D_0 \rightarrow {}^7F_2 > {}^7F_1 > {}^7F_4$ for Eu–EDA. This result indicates that the different conformation of the ligands of the Eu–DAP and Eu–EDA complexes has an effect on the $\beta_{0J'}$ values. Concerning the temperature dependence of $\beta_{0J'}$ displayed in Fig. 8c, it is possible to observe that for Eu–EDA these values do not depend on the temperature. However, for Eu–DAP β_{01} remains almost constant between 13.5 and 120 K, then decreasing almost 50% with increasing temperature, due to the inversion of the relative intensities of the $^5D_0 \rightarrow {}^7F_1$ and $^5D_0 \rightarrow {}^7F_4$ transitions; phenomenon not observed in the Eu–EDA spectra for $T > 120$ K.

4. Conclusions

All complexes have ten coordinated europium ions, with three bidentated nitrate ligands. However, the presence of different macrocyclic ligands allows different conformations: Eu-DAP and Eu-EDA are better described as a spherocorona, while Eu-OPDA is closer to a tetradecahedron.

Of the three studied complexes, the antenna effect was observed for Eu-DAP and Eu-EDA, being greater for the former. Due to the absence of an inversion center in the complexes, the emission spectra of Eu–DAP and Eu–EDA at room temperature show more intense $^5D_0 \rightarrow {}^7F_2$ emission peaks as compared to $^5D_0 \rightarrow {}^7F_1$, with relatively high R/O ratios. With the decrease of temperature these $^5D_0 \rightarrow {}^7F_{1,2}$ emissions become enhanced and resolved.

The calculated Judd–Ofelt intensity parameters (Ω_2 and Ω_4) at room temperature, suggest a moderate covalent bond between the metal center and the ligand. Moreover, the $^5D_0$ lifetime for Eu–DAP is highly temperature dependent. The Ω_2 and radiative lifetime (τ_R) values for Eu–DAP have a complementary behavior over all the studied temperature range, and are related to the structural changes around the lanthanide ion.

Acknowledgements

The authors thank Proyecto FONDECYT 1160106 and Proyecto Anillo CONICYT ACT 1404 grants for financial support. ESS, PFC, VPG, DVY are also members of CEDENNA, Financiamiento Basal, FB0807. PFC also thanks FONDECYT for postdoctoral grant 3170186. The authors also acknowledge CNPq and FAPEG in Brazil. Powered@NLHPC: This research was partially supported by the supercomputing infrastructure of the NLHPC (ECM–02).

Appendix A. Supporting information

Supplementary data associated with this article can be found in the online version at https://doi.org/10.1016/j.jlumin.2018.06.022.

References

[1] D.N. Woodruff, R.E.P. Winpenny, R.A. Layfield, Lanthanide single-molecule magnets, Chem. Rev. 113 (2013) 5110–5148, http://dx.doi.org/10.1021/cr400018q.

[2] L. Armelao, S. Quici, F. Barigelletti, G. Accorsi, G. Bottaro, M. Cavazzini, E. Tondello, Design of luminescent lanthanide complexes: from molecules to highly efficient photo-emitting materials, Coord. Chem. Rev. 254 (2010) 487–505, http://dx.doi.org/10.1016/j.ccr.2009.07.025.

[3] V. Alexander, Design and synthesis of macrocyclic ligands and their complexes of lanthanides and actinides, Chem. Rev. 95 (1995) 273–342, http://dx.doi.org/10.1021/cr00034a002.

[4] J. Lisowski, P. Starynowicz, The macrocyclic mononuclear lanthanide complexes derived from 2,6-diformyl-4-methylphenol and 1,3-diamino-2-hydroxypropane, Polyhedron 18 (1998) 443–450, http://dx.doi.org/10.1016/S0277-5387(98)00316-7.

[5] E. Spodine, Y. Moreno, M.T. Garland, O. Pena, R. Baggio, Molecular structure and magnetic properties of [Gd(LH4)(NO3)2(H2O)]NO3(H2O)2, [Sm(LH4)(NO3)2(H2O)]NO3 (H2O)1.5(CH3OH)0.5 and [Cu2(LH2)(H2O)2](NO3)2 complexes (LH4: schiff base ligand derived from 4-methyl-2,6-diformylphenol and 1,3-diaminopropanol), Inorg. Chim. Acta 309 (2000) 57–64, http://dx.doi.org/10.1016/S0020-1693(00)00232-2.

[6] H.C. Aspinall, Chiral lanthanide complexes: coordination chemistry and applications, Chem. Rev. 102 (2002) 1807–1850, http://dx.doi.org/10.1021/cr010288q.

[7] P.A. Vigato, S. Tamburini, The challenge of cyclic and acyclic schiff bases and related derivatives, Coord. Chem. Rev. 248 (2004) 1717–2128, http://dx.doi.org/10.1016/j.cct.2003.09.003.

[8] B. Makhinson, A.K. Duncan, A.R. Elam, A. de Bettencourt-Dias, C.D. Medley, J.E. Smith, E.J. Werner, Turning on lanthanide luminescence via nanoencapsulation, Inorg. Chem. 52 (2013) 6311–6318, http://dx.doi.org/10.1021/ic3022722.

[9] A.K. Duncan, C.N. McBride, T.G.R. Benjamin, M.P. Madsen, K.T. Bowers, A. de Bettencourt-Dias, E.J. Werner, Tuning the structural and lanthanide luminescence properties of macrocyclic tetraiminodiphenolate eEuropium(III) complexes, Polyhedron 114 (2016) 451–458, http://dx.doi.org/10.1016/j.poly.2016.03.052.

[10] L.D. Carlos, R.A.S. Ferreira, V. de, Z. Bermudez, S.J.L. Ribeiro, Lanthanide-containing light-emitting organic-inorganic hybrids: a bet on the future, Adv. Mater. 21 (2009) 509–534, http://dx.doi.org/10.1002/adma.200801635.

[11] K. Binnemans, Lanthanide-based luminescent hybrid materials, Chem. Rev. 109 (2009) 4283–4374, http://dx.doi.org/10.1021/cr8003983.

[12] E. Kasprzycka, V.A. Trush, V.M. Amirkhanov, L. Jerzykiewicz, O.L. Malta, J. Legendziewicz, P. Gawryszewska, Contribution of energy transfer from the singlet state to the sensitization of Eu^{3+} and Tb^{3+} luminescence by sulfonylamidophosphates, Chem. - A Eur. J. 23 (2017) 1318–1330, http://dx.doi.org/10.1002/chem.201603767.

[13] V.F. Plyusnin, A.S. Kupryakov, V.P. Grivin, A.H. Shelton, I.V. Sazanovich, A.J.H.M. Meijer, J. a Weinstein, M.D. Ward, Photophysics of 1,8-naphthalimide/Ln(III) dyads (Ln = Eu, Gd): naphthalimide → Eu(III) energy-transfer from both singlet and triplet states, Photochem. Photobiol. Sci. 12 (2013) 1666–1679, http://dx.doi.org/10.1039/c3pp50109d.

[14] J. Andres, A.-S. Chauvin, Energy transfer in coumarin-sensitised lanthanide luminescence: investigation of the nature of the sensitiser and its distance to the lanthanide ion, Phys. Chem. Chem. Phys. 15 (2013) 15981, http://dx.doi.org/10.1039/c3cp52279b.

[15] M. Kleinerman, Energy migration in lanthanide chelates, J. Chem. Phys. 51 (1969) 2370–2381, http://dx.doi.org/10.1063/1.1672355.

[16] H.B. Kagan, Introduction: frontiers in lanthanide chemistry, Chem. Rev. 102 (2002) 1805–1806.

[17] J.-C.G. Bünzli, Review: lanthanide coordination chemistry: from old concepts to coordination polymers, J. Coord. Chem. 67 (2014) 3706–3733, http://dx.doi.org/10.1080/00958972.2014.957201.

[18] K. Binnemans, Interpretation of Europium(III) spectra, Coord. Chem. Rev. 295 (2015) 1–45, http://dx.doi.org/10.1016/j.ccr.2015.02.015.

[19] D. Parker, Luminescent lanthanide sensors for pH, pO2 and selected anions, Coord. Chem. Rev. 205 (2000) 109–130, http://dx.doi.org/10.1016/S0010-8545(00)00241-1.

[20] J.A. Peters, J. Huskens, D.J. Raber, Lanthanide induced shifts and relaxation rate enhancements, Prog. Nucl. Magn. Reson. Spectrosc. 28 (1996) 283–350, http://dx.doi.org/10.1016/0079-6565(95)01026-2.

[21] A.S. Merbach, L. Helm, E. Toth, The Chemistry of Contrast Agents in Medical Magnetic Resonance Imaging, 2nd ed., New York, 2013.

[22] C.H. Evans, Biochemistry of the Lanthanides, Springer US, Boston, MA, 1990, http://dx.doi.org/10.1007/978-1-4684-8748-0.

[23] É. Tóth, L. Burai, A.E. Merbach, Similarities and differences between the isoelectronic GdIII and EuII complexes with regard to MRI contrast agent applications, Coord. Chem. Rev. 216–217 (2001) 363–382, http://dx.doi.org/10.1016/S0010-8545(01)00312-5.

[24] J.-C.G. Bünzli, S. Comby, A.-S. Chauvin, C.D.B. Vandevyver, New opportunities for lanthanide luminescence, J. Rare Earths 25 (2007) 257–274, http://dx.doi.org/10.1016/S1002-0721(07)60420-7.

[25] S.V. Eliseeva, J.-C.G. Bünzli, Lanthanide luminescence for functional materials and bio-sciences, Chem. Soc. Rev. 39 (2010) 189–227, http://dx.doi.org/10.1039/B905604C.

[26] E.J. New, D. Parker, D.G. Smith, J.W. Walton, Development of responsive lanthanide probes for cellular applications, Curr. Opin. Chem. Biol. 14 (2010) 238–246, http://dx.doi.org/10.1016/j.cbpa.2009.10.003.

[27] J.C.G. Bünzli, S.V. Eliseeva, Lanthanide NIR luminescence for telecommunications, bioanalyses and solar energy conversion, J. Rare Earths 28 (2010) 824–842, http://dx.doi.org/10.1016/S1002-0721(09)60208-8.

[28] D.S. Kumar, V. Alexander, Macrocyclic complexes of lanthanides in identical ligand frameworks part 1. Synthesis of lanthanide(III) and yttrium(III) complexes of an 18-membered dioxatetraaza macrocycle, Inorg. Chim. Acta 238 (1995) 63–71, http://dx.doi.org/10.1016/0020-1693(95)04687-5.

[29] R.D. Archer, H. Chen, L.C. Thompson, Synthesis, characterization, and luminescence of Europium(III) Schiff Base complexes 1 a, Inorg. Chem 37 (1998) 2089–2095, http://dx.doi.org/10.1021/ic960244d.

[30] S. Som, S.K. Sharma, T. Shripathi, Influences of doping and annealing on the structural and photoluminescence properties of Y2O3 nanophosphors, J. Fluoresc. 23 (2013) 439–450, http://dx.doi.org/10.1007/s10895-013-1160-7.

[31] V. Blum, R. Gehrke, F. Hanke, P. Havu, V. Havu, X. Ren, K. Reuter, M. Scheffler, Ab initio molecular simulations with numeric atom-centered orbitals, Comput. Phys. Commun. 180 (2009) 2175–2196, http://dx.doi.org/10.1016/j.cpc.2009.06.022.

[32] J.P. Perdew, K. Burke, M. Ernzerhof, Generalized gradient approximation made simple, Phys. Rev. Lett. 77 (1996) 3865–3868, http://dx.doi.org/10.1103/PhysRevLett.77.3865.

[33] E. van Lenthe, E.J. Baerends, J.G. Snijders, Relativistic total energy using regular approximations, J. Chem. Phys. 101 (1994) 9783–9792, http://dx.doi.org/10.1063/1.467943.

[34] M. Llunell, D. Casanova, J. Cirera, P. Alemany, S. Alvarez, SHAPE (version 2.1), SHAPE (Version 2.1). (n.d.)Barcelona, 2013.

[35] S. Alvarez, P. Alemany, D. Casanova, J. Cirrea, M. Llunell, D. Avnir, Shape maps and polyhedral interconversion paths in transition metal chemistry, Coord. Chem. Rev. 249 (2005) 1693–1708, http://dx.doi.org/10.1016/j.ccr.2005.03.031.

[36] P. Bag, U. Flörke, K. Nag, Synthesis and structural characterization of lanthanide (III) nitrate complexes of a tetraiminodiphenol macrocycle in the solid state and in solution, Dalton Trans. (2006) 3236–3248, http://dx.doi.org/10.1039/b516306d.

[37] K. Nakamoto, Infrared and Raman spectra of inorganic and coordination compounds: Part B: applications in coordination, Organomet. Bioinorg. Chem. (2008), http://dx.doi.org/10.1002/9780470405888.

[38] P. Kubelka, F. Munk, Ein Beitrag zur Optik der Farbanstriche, Z. Für Tech. Phys. 12 (1931) 593–601.

[39] C. Adachi, M.A. Baldo, S.R. Forrest, Electroluminescence mechanisms in organic light emitting devices employing a europium chelate doped in a wide energy gap bipolar conducting host, J. Appl. Phys. 87 (2000) 8049, http://dx.doi.org/10.1063/1.373496.

[40] J. Roncali, Synthetic principles for bandgap control in linear π-conjugated systems, Chem. Rev. 97 (1997) 173–206, http://dx.doi.org/10.1021/cr950257t.

[41] J. Roncali, Molecular engineering of the band gap of π-conjugated systems: facing technological applications, Macromol. Rapid Commun. 28 (2007) 1761–1775, http://dx.doi.org/10.1002/marc.200700345.

[42] T.-W. Duan, B. Yan, Hybrids based on lanthanide ions activated yttrium metal–organic frameworks: functional assembly, polymer film preparation and luminescence tuning, J. Mater. Chem. C 2 (2014) 5098, http://dx.doi.org/10.1039/c4tc00414k.

[43] F.A. de Jesus, S.T.S. Santos, J.M.A. Caiut, V.H.V. Sarmento, Effects of thermal treatment on the structure and luminescent properties of Eu3+ doped SiO2–PMMA hybrid nanocomposites prepared by a sol–gel process, J. Lumin. 170 (2016) 588–593, http://dx.doi.org/10.1016/j.jlumin.2015.05.030.

[44] J.C. Boyer, F. Vetrone, J.A. Capobianco, A. Speghini, M. Bettinelli, Variation of fluorescence lifetimes and Judd-Ofelt parameters between Eu 3+ doped bulk and nanocrystalline cubic Lu 2 O 3, J. Phys. Chem. B 108 (2004) 20137–20143, http://dx.doi.org/10.1021/jp0480504.

[45] O.L. Malta, L.D. Carlos, Intensities of 4f-4f transitions in glass materials, Quim. Nova 26 (2003) 889–895.

[46] L.D. Carlos, R.A. Sá Ferreira, V. De Zea Bermudez, C. Molina, L.A. Bueno, S.J.L. Ribeiro, , White light emission of Eu3+ based hybrid xerogels, Phys. Rev. B 60 (1999) 10042–10053, http://dx.doi.org/10.1103/PhysRevB.60.10042.

[47] Y.-J. Li, X. Yu, X. Wang, M. Yang, Lanthanide (Eu3+, Tb3+) functionalized SBA-15 through modified hexafluoroacetylacetone linkage: covalently bonding construction, physical characterization, and luminescent properties, J. Mater. Res. 29 (2014) 675–683, http://dx.doi.org/10.1557/jmr.2014.33.

[48] Y.C. Ratnakaram, V.R. Prasad, S. Babu, V.V. Ravi Kanth Kumar, Luminescence performance of Eu3+-doped lead-free zinc phosphate glasses for red emission, Bull. Mater. Sci. 39 (2016) 1065–1072, http://dx.doi.org/10.1007/s12034-016-1249-0.

[49] H. Liang, F. Xie, X. Ren, Y. Chen, B. Chen, F. Guo, Temperature dependent luminescence of a europium complex incorporated in poly(methyl methacrylate), Spectrochim. Acta - Part A Mol. Biomol. Spectrosc. 116 (2013) 317–320, http://dx.doi.org/10.1016/j.saa.2013.07.034.

[50] B.R. Judd, Optical absorption intensities of rare-earth ions, Phys. Rev. 127 (1962) 750–761, http://dx.doi.org/10.1103/PhysRev.127.750.

[51] G.S. Ofelt, Intensities of crystal spectra of rare-earth ions, J. Chem. Phys. 37 (1962) 511, http://dx.doi.org/10.1063/1.1701366.

[52] K. Rademaker, Rare Earth-Doped Alkali-Lead-Halide Laser Crystals of Low- Phonon Energy, Hamburg University, 2005.

[53] W. Krupke, Radiative transition probabilities within the 4f3 ground configuration of Nd:YAG, IEEE J. Quantum Electron. 7 (1971) 153–159, http://dx.doi.org/10.1109/JQE.1971.1076623.

[54] K.J.B.M. Nieuwesteeg, Judd-Ofelt intensity parameters in europium-, terbium- and thulium-activated, Philips J. Res. 44 (1989) 385–406.
[55] W.T. Carnall, P.R. Fields, B.G. Wybourne, Spectral intensities of the trivalent lanthanides and actinides in solution. I. Pr3+, Nd3+, Er3+, Tm3+, and Yb3+, J. Chem. Phys. 42 (1965) 3797, http://dx.doi.org/10.1063/1.1695840.
[56] S. Biju, D.B.A. Raj, M.L.P. Reddy, B.M. Kariuki, Synthesis, crystal structure, and luminescent properties of novel Eu 3+ heterocyclic β-diketonate complexes with bidentate nitrogen donors, Inorg. Chem. 45 (2006) 10651–10660, http://dx.doi.org/10.1021/ic061425a.
[57] P.P. Lima, R.A. Sá Ferreira, R.O. Freire, F.A. Almeida Paz, L. Fu, S. Alves, L.D. Carlos, O.L. Malta, Spectroscopic study of a UV-photostable organic-inorganic hybrids incorporating an Eu3+ β-diketonate complex, ChemPhysChem 7 (2006) 735–746, http://dx.doi.org/10.1002/cphc.200500588.
[58] C. Molina, K. Dahmouche, Y. Messaddeq, S.J. Ribeiro, M.A. Silva, V. de Zea Bermudez, L. Carlos, Enhanced emission from Eu(III) β-diketone complex combined with ether-type oxygen atoms of di-ureasil organic–inorganic hybrids, J. Lumin. 104 (2003) 93–101, http://dx.doi.org/10.1016/S0022-2313(02)00684-1.
[59] R. Reisfeld, Spectra and energy transfer of rare earths in inorganic glasses, Struct. Bond. (1973) 53–98, http://dx.doi.org/10.1007/3-540-06125-8_2.
[60] R. Shukla, S.K. Gupta, V. Grover, V. Natarajan, A.K. Tyagi, The role of reaction conditions in the polymorphic control of Eu 3+ doped YInO 3: structure and size sensitive luminescence, Dalton Trans. 44 (2015) 10628–10635, http://dx.doi.org/10.1039/C4DT02717E.
[61] S. Som, A.K. Kunti, V. Kumar, V. Kumar, S. Dutta, M. Chowdhury, S.K. Sharma, J.J. Terblans, H.C. Swart, Defect correlated fluorescent quenching and electron phonon coupling in the spectral transition of Eu3+ in CaTiO3 for red emission in display application, J. Appl. Phys. 115 (2014) 193101, http://dx.doi.org/10.1063/1.4876316.
[62] M.T. Berry, P.S. May, H. Xu, Temperature dependence of the Eu 3+ 5 D 0 lifetime in europium Tris(2,2,6,6-tetramethyl-3,5-heptanedionato), J. Phys. Chem. 100 (1996) 9216–9222, http://dx.doi.org/10.1021/jp953702x.